Appl. Phys. B 58, 519–528 (1994)

Applied Physics B Lasers and Optics



# Wide- and Narrow-Band Saturated Fluorescence Measurements of Hydroxyl Concentration in Premixed Flames from 1 bar to 10 bar

**C. D. Carter*, N. M. Laurendeau**

Flame Diagnostics Laboratory, School of Mechanical Engineering, Purdue University, West Lafayette, IN 47907, USA
(Fax: + 1-317/494-0539, e-mail: laurende@ecn.purdue.edu)

Received 13 August 1993/Accepted 17 January 1994

**Abstract.** We have studied the use of wide-band detection in conjunction with saturation of a rovibronic transition of OH within its $A^2\Sigma^+$-$X^2\Pi(0,0)$ band. For wide-band detection, in which fluorescence is detected from the entire excited rotational manifold, the fluorescence yield is sensitive to collisions in two ways. First, it is sensitive to the ratio of rate coefficients describing rotational energy transfer and electronic quenching; this ratio determines the number of neighboring rotational levels that are populated during the laser pulse. Second, the fluorescence yield can vary with the total collisional rate coefficient; only after a sufficient number of collisions, corresponding to $\approx$2.5 ns in an atmospheric flame, does the rotational manifold reach steady state. We also compare measurements employing wide-band (detecting the $R_1$ and $R_2$ branches) and narrow-band (detecting a single transition) saturated fluorescence of OH. Over a wide range of conditions – obtained by varying the equivalence ratio, temperature, $N_2$ dilution, and pressure – the wide- and narrow-band fluorescence techniques compare well. Given this good agreement, wide-band saturated fluorescence could be especially useful for analyzing atmospheric flames with XeCl-excimer lasers; one can potentially obtain 2–D images of OH which have a high signal-to-noise ratio and a reduced sensitivity to laser irradiance and quenching.

**PACS:** 34.50.Ez, 42.65.Ft, 82.40.Py

Laser-saturated fluorescence was first proposed as a general-purpose diagnostic by Piepmeier [1] and later as a combustion diagnostic by Daily [2]. Since that time it has been applied to diatomic species in sub-atmospheric and atmospheric flames [3–7]. Its principal advantage over linear fluorescence is that the derived signal has reduced sensitivity to collisional quenching and laser power. Because saturation results in the maximum population in the directly-excited rovibronic state, one can detect fluorescence from this level only, thereby allowing measurements of low concentrations ($< 10^{14}$ cm$^{-3}$) even in sooting or particle-laden flames [8]. Though initially thought to be applicable only in low-pressure environments, saturated fluorescence has recently been demonstrated in flames exceeding several bar [9–11].

Initially experimenters employed a wide-band detection scheme for the saturated fluorescence measurements of $C_2$, MgO, CH, and CN in atmospheric flames [12–14]; that is, the fluorescence was detected from many rovibronic levels (i.e., using a complete band or bandhead). Wide-band detection of these species, with the exception of CH, was necessitated by the difficulty of spectrally isolating the laser-excited rovibronic state. Using a detailed transient model for hydroxl (OH), Lucht and Laurendeau [15] showed that to obtain a Boltzmann (i.e., equilibrium) population distribution among the excited-state rotational levels *during* the laser pulse, the ratio of the rate coefficients for rotational energy transfer (from the directly-excited state) to electronic quenching should be at least 100. After determining experimentally that the excited rotational manifold of hydroxyl (in sub-atmospheric flames) was not in equilibrium during the laser pulse, Lucht et al. [16] proposed (i) monitoring only the directly-excited state (instead of the whole manifold) and (ii) using the so-called balanced cross-rate model to relate the measured fluorescence (from the single state) to the ground-state population. Subsequent experiments verified the accuracy of this model for low-pressure environments [3, 6].

Even in cases for which rotational equilibrium is not attained, monitoring the entire rovibronic manifold is attractive, since this would significantly increase the signal level. It could also simplify detection of the fluorescence, since interference or color-glass filters could replace the spectrometer. In addition, with adequate saturation within the laser sheet, one could obtain quantitative 2–D saturated fluorescence images [17, 18]. For

* Currently with Systems Research Laboratories, Inc. (A Division of Arvin/Calspan), 2800 Indian Ripple Rd., Dayton, OH 45440–3696, USA

diatomics with smaller rotational constants, e.g., NO and CN, saturation of selected rovibronic transitions is possible [14, 19], but isolating a single fluorescence transition is not practical. On the other hand, with wide-band detection one is monitoring collisionally-populated states in addition to the directly-coupled state; thus, the fluorescence signal will be sensitive to collisions in ways not encountered when using narrow-band detection.

In this paper we investigate the potential for quantitative concentration measurements using the wide-band saturated fluorescence technique at pressures from 1 bar to 10 bar. We develop appropriate theory for understanding the sensitivity of wide-band saturated fluorescence to collisions, and we compare wide- and narrow-band fluorescence measurements of hydroxyl over a broad range of conditions. For the wide-band measurements, we detect fluorescence from the $R_1$ and $R_2$ branches of the (0, 0) band (using a monochromator), while for the narrow-band measurements, we isolate fluorescence from the state directly pumped by the laser ($v'=0$, $N'=8$). In both cases we image the fluorescence onto the monochromator entrance slit, thereby discriminating against the low-intensity wings of the beam; in this way we focus on the effect of collisions on the wide-band signal relative to the effect on the narrow-band signal. Nonetheless, our conclusions do not pertain solely to point measurements; they are also valid for 2-D saturated fluorescence imaging. Furthermore, the theory and modelling can be extended to wide-band measurement of other diatomic molecules.

## 1 Theory and Modelling

To describe the differences between narrow-band and wide-band saturated fluorescence, we first derive approximate expressions for the wide-band method using the governing rate equations. In conjunction with this, we employ a time-dependent model which uses 56 rate equations to describe the rotational-level populations within the $A^2\Sigma^+$-$X^2\Pi(0,0)$ system [20]. To model the spatial dependence of the laser irradiance, we use both Gaussian and quasi-Lorentzian functions; we define the latter as [10]

$$f(r) \equiv \frac{1}{[1+(r/w)^2]^{2.2}}, \tag{1}$$

where $r$ is the radius from the beam centerline and $w$ is the beam half width. To reduce the sensitivity of the saturated fluorescence measurements to quenching and laser energy, we normally collect fluorescence from a thin slice along the central chord of the volume probed by the laser (e.g., an 80 μm slice in a beam with a 200 μm FWHM). Thus, to accurately model our experiment, we employ a 1-D radial integration of the excited-state populations. This procedure using (1) provides a good match with the measured dependence of fluorescence on laser energy [10]. Temporal integration of the system is performed with the solver LSODE [21], while spatial integration (for the excited-state populations) is approximated with appropriate quadrature formulas [20]. The FORTRAN package was executed on an 80486 IBM-compatible PC, with typical solution times of $\approx 1$ min.

The population of the upper laser-coupled rovibronic state (denoted by $u$) is described with the following rate equation

$$\frac{dN_u}{dt} = N_l W_{lu} - N_u[W_{ul} + Q_e] + \sum_{j\neq u} [N_j Q_r(j, u) - N_u Q_r(u, j)], \tag{2}$$

where spontaneous emission and vibrational energy transfer ($v'=0\rightarrow 1$) have been neglected due to their small magnitudes. $N_l$ and $N_u$ are the number densities of the ground and excited rovibronic states, respectively, and $W_{lu}$ and $W_{ul}$ are the respective rate coefficients for absorption and stimulated emission. The collisional rate coefficients are represented by $Q_e$ for electronic quenching and $Q_r(m, n)$ for Rotational Energy Transfer (RET) from rovibronic state $m$ to $n$ [20, 22]. For the manifold of collisionally-populated states (i.e., those populated only by RET) within $v'=0$, we have the expression

$$\frac{dN_c}{dt} = N_u \sum_{j\neq u} Q_r(u, j) - \sum_{j\neq u} N_j[Q_e + Q_r(j, u)], \tag{3}$$

where $N_c \equiv \sum_{j\neq u} N_j$. For simplicity, especially for the analytical development, we assume that $Q_e$ is independent of the rotational state. This is an approximation even at flame temperatures [23]; however, for our purposes, including a dependence on rotational state for $Q_e$ is not warranted by the accuracy and availability of data describing high-temperature quenching *or* RET. To obtain a simple analytical solution for the temporal dependence of the manifold population, we define a mean backward rate coefficient,

$$\overline{Q}_r(c, u) \equiv \frac{1}{N_c} \sum_{j\neq u} N_j Q_r(j, u), \tag{4}$$

which we will assume to be independent of the distribution within the collisionally-populated manifold. In reality, of course, $\overline{Q}_r(c, u)$ is a function of the distribution, since the individual $Q_r(m, n)$ decrease with increasing energy separation between levels $m$ and $n$. Early in the laser pulse the population of the manifold is in energy levels close to the directly-excited level; consequently, $\overline{Q}_r(c, u)$ is larger than at later times.

Nonetheless, by substituting (4) into (3), we can estimate the time necessary for the rotational manifold to reach steady state *after* level $u$ reaches steady state. The resulting solution for $N_c$ is

$$N_c(t) = \frac{N_u^{ss} Q_{r,u}\{1 - \exp[-(Q_e + Q_{r,c})t]\}}{(Q_e + Q_{r,c})}, \tag{5}$$

where we have used $Q_{r,u}$ for $Q_r(u, c) \equiv \sum_{j\neq u} Q_r(u, j)$ and $Q_{r,c}$ for $\overline{Q}_r(c, u)$. The manifold will approach steady state,

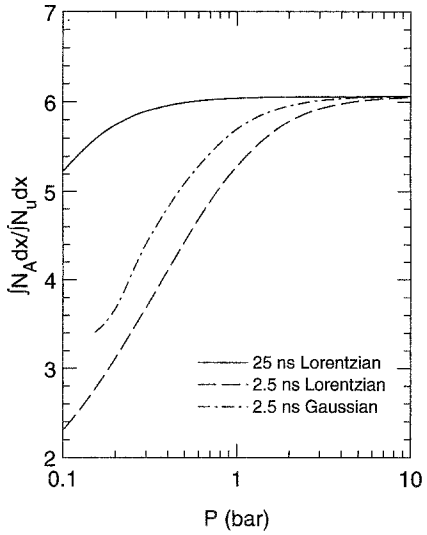


**Fig. 1.** Peak spatially integrated population in the $A$ state (i.e., the peak temporal value of $N_A = N_c + N_u$), normalized with peak $N_u$, vs pressure. The spatial dependence of the laser irradiance is modeled with both quasi-Lorentzian and Gaussian profiles. The temporal dependence in the three cases is modelled with a Gaussian function. The associated temporal widths are 2.5 ns and 25 ns (FWHM) for the quasi-Lorentzian spatial profile and 2.5 ns (FWHM) for the Gaussian spatial profile.

$$N_c^{ss} = \frac{N_u^{ss} Q_{r,u}}{Q_e + Q_{r,c}} = \frac{N_u^{ss}}{Q_e/Q_{r,u} + Q_{r,c}/Q_{r,u}}, \quad (6)$$

with a characteristic time $t_c = (Q_e + Q_{r,c})^{-1}$. Thus, even when level $u$ is well saturated, the wide-band fluorescence yield is sensitive to (*i*) the sum $Q_e + Q_{r,c}$ when the laser pulse is short compared to this characteristic collision time, and (*ii*) the collisional branching ratio $Q_{r,u}/Q_e$.

The ratio $N_u^{ss}/N_c^{ss}$ is a measure of rotational *thermalization*. Zizak et al. [24] recorded this ratio for several excited rovibronic states within $v' = 0$. For a $CH_4$/air flame and a rotational quantum number of $N' = 8$ (in the $A$ state), they found $N_u^{ss}/N_c^{ss} \cong 0.2$. Using our dynamic rate-equation model [20], we have deduced a ratio of $Q_{r,u}/Q_e = 8$ (while they estimated a value of 6.7) from $N_u^{ss}/N_c^{ss} = 0.2$. Assuming an atmospheric rate coefficient of $Q_e = 0.5 \times 10^9\ s^{-1}$ [25] gives $Q_{r,u} = 4 \times 10^9\ s^{-1}$. Using these parameters with our dynamic model, we find that over a wide range of time during excitation, $Q_{r,c}$ varies from $\approx 0.5 \times 10^9\ s^{-1}$ (early during excitation) to $0.3 \times 10^9\ s^{-1}$, which is the steady-state value from (6). Therefore, at atmospheric pressure, using $Q_{r,c} = 0.4 \times 10^9\ s^{-1}$, we calculate with (5) that $N_c$ reaches 90% of its steady-state value $\approx 2.5$ ns after level $u$ reaches steady state.

Employing our dynamic rate-equation model, we show in Fig. 1 the influence of pressure (or total collision rate, $Q_e + Q_{r,c}$) on the fluorescence yield. The peak, normalized, spatially integrated $A$-state population – where $N_A = N_u + N_c$ – is plotted versus pressure for two different laser pulse widths, 2.5 ns and 25 ns (FWHM), with both temporal profiles described by Gaussian functions. These temporal widths were chosen to approximate pulses produced by our Nd:YAG/dye laser system

**Table 1.** Parameters for dynamic rate equation model

| | |
|---|---|
| $T$ | 1750 K |
| Coupled rovibronic states | $N'' = 8$, $J'' = 8.5$; $N' = 8$, $J' = 8.5$ |
| $W_{lu}$ (maximum value) | $10^{13}\ s^{-1}$ with $\Delta t_L = 2.5$ ns (FWHM)<br>$10^{12}\ s^{-1}$ with $\Delta t_L = 25$ ns (FWHM) |
| Rovibronic levels | $A^2\Sigma^+(v' = 0)$: 29 levels, $N' = 0$ to 14<br>$X^2\Pi(v'' = 0)$: 26 levels, $N'' = 1$ to 13<br>(no $\Lambda$ doubling) |
| $k_{Q_e}$ | $0.5 \times 10^9\ s^{-1}\ bar^{-1}$, independent of rotational state |
| $Q_r(m, n)$ | modified exponential gap scaling for upward ($E_n > E_m$) RET;<br>detailed balancing for downward RET [20, 22] |
| $Q_r(u, c)$ | 8 $Q_e$, except where noted (e.g., Fig. 2) |

($\Delta t_L \cong 2.5$ ns, FWHM) and that produced by a XeCl-excimer system (25 ns, FWHM). The peak rate coefficient for absorption, $W_{lu}$, was chosen to ensure a maximum degree of saturation of >95% for all cases; nonetheless, the dependence on peak saturation is largely removed through normalization with $N_u$. The collisional rate coefficients were derived by scaling linearly with pressure the atmospheric values given above. The input parameters for our dynamic rate-equation model are summarized in Table 1.

For the 2.5 ns excitation pulse, the $A$-state population at atmospheric pressure is only 6% to 12% below the steady-state value. This difference decreases with higher pressures, as the increased number of collisions acts to fill the rotational manifold. For a Gaussian spatial profile, a smaller fraction of the laser energy is in the wings of the beam where the fluorescence is linear or near linear. With a higher degree of saturation – averaged over the spatial extent of the beam – the population reaches steady state at lower pressures, when compared to the quasi-Lorentzian beam. With a 2.5 ns pulse, the fluorescence exhibits a small sensitivity to the total collision rate $Q_e + Q_{r,c}$ at atmospheric pressure. However, the sensitivity to $Q_e + Q_{r,c}$ has disappeared by 1 bar when using a 25 ns laser pulse. An additional effect of saturation is temporal broadening of the fluorescence profile; thus, during saturation the excited rotational manifold will have more time to reach steady state than one would expect from the temporal half width of the laser irradiance profile.

We next examine in more detail the sensitivity of the $A$-state population under steady-state conditions, $N_A^{ss}$, to the collisional branching ratio $Q_{r,u}/Q_e$. When $Q_{r,u}$ increases relative to $Q_e$, the population in the neighboring (collisionally-populated) states also increases; thus, the wide-band fluorescence yield is sensitive to the ratio $Q_{r,u}/Q_e$. However, as this ratio becomes very large, we expect that the excited-state population will approach a Boltzmann distribution *during* the laser pulse, as reported by Lucht and Laurendeau [15]. At this limiting distribution, the sensitivity of $N_c^{ss}$ (and thus the fluorescence yield, assuming complete saturation) to $Q_{r,u}/Q_e$ is zero. Of

particular interest is the sensitivity of $N_A^{ss}$ to $Q_{r,u}/Q_e$ for the hydroxyl radical. To simplify (6), we use the relative equilibrium populations of levels $u$ and $c$, $N_u^e$ and $N_c^e$, respectively, and the approximation [19]

$$\frac{\overline{Q}_r(c,u)}{Q_r(u,c)} \cong \frac{N_u^e}{N_c^e}, \tag{7}$$

which would hold exactly if the manifold were a single state. In reality, away from equilibrium, $Q_{r,c}/Q_{r,u}$ is larger than $N_u^e/N_c^e$. Substitution of (7) into (6) yields

$$N_c^{ss} \cong \frac{N_u^{ss}}{(Q_e/Q_{r,u})+(N_u^e/N_c^e)} \tag{8}$$

and

$$\frac{N_A^{ss}}{N_u^{ss}} \cong \frac{1}{(Q_e/Q_{r,u})+(N_u^e/N_c^e)} + 1. \tag{9}$$

The sensitivity of the wide-band fluorescence yield to RET is then given by

$$\frac{d(N_A^{ss}/N_u^{ss})}{d(Q_{r,u}/Q_e)} \cong \frac{1}{[1+(N_u^e/N_c^e)\,(Q_{r,u}/Q_e)]^2}. \tag{10}$$

Equation (8) indicates that to obtain a Boltzmann relationship between the directly-coupled state and the manifold of collisionally-populated states, one needs $Q_e/Q_{r,u} \ll N_u^e/N_c^e$. Since the fraction of population within an individual rotational level, that is the Boltzmann fraction $F_B$, is typically small compared to unity, we can use the approximation $N_u^e/N_c^e \cong F_{Bu}$. Therefore, a Boltzmann distribution results from the condition

$$Q_{r,u}/Q_e \gg 1/F_{Bu}. \tag{11}$$

Typically, $F_{Bu}=0.05$ for OH $A^2\Sigma^+(v=0, N=8)$ at flame temperatures; thus, we conclude that $Q_{r,u}$ must be *much greater* than $20 \times Q_e$ to achieve rotational equilibrium.

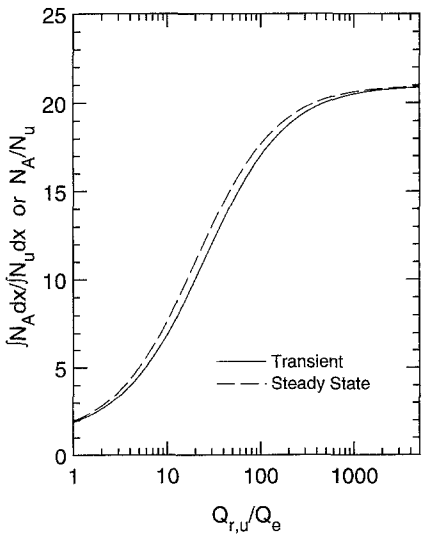


**Fig. 2.** Normalized population in the $A$ state – using a pressure of 1 bar and a temporal width of 25 ns – vs the ratio $Q_{r,u}/Q_e$ from the transient model (using the peak values of $\int N_A dx$ and $\int N_u dx$) and from the steady-state solution given by (9)

That is, many RET collisions, perhaps 200 per quenching collision, are required to redistribute the *laser-induced* population and obtain a Boltzmann distribution (between level $u$ and the manifold $c$) during laser excitation. Since $Q_{r,u}/Q_e \cong 8$, we conclude that (*i*) the OH $A^2\Sigma^+$ state will have a non-Boltzmann distribution during the laser pulse, and (*ii*) the wide-band fluorescence yield will be sensitive to the ratio $Q_{r,u}/Q_e$. This first point was illustrated by Zizak et al. [24]. The second point is illustrated in Fig. 2, which shows the normalized $A$-state population versus $Q_{r,u}/Q_e$ for a pressure of 1 bar. In addition to the steady-state result given by (9), we have used the dynamic model with a pulse duration of 25 ns (to ensure that the rotational manifold has reached steady state). For the transient solution, the spatially-integrated values have been used, though the results are insensitive to the laser spatial profile for a 25 ns excitation pulse.

With molecules having smaller rotational constants (e.g., NO), the rotational levels are closer in energy, and consequently one might expect $Q_{r,u}/Q_e$ to be larger; however, this would likely be offset by the concomitant smaller Boltzmann fraction (again due to the smaller rotational constant). Thus, the aforementioned conclusions (*i* and *ii*) are probably valid for most molecules under most circumstances. One notable exception might be NO with a collision partner of $N_2$ (at low temperatures), Ar, or He, since these species are efficient at RET [26, 27] but inefficient at quenching NO $A^2\Sigma^+$ [28].

Finally, we note that with both wide- and narrow-band saturated fluorescence, a relatively large fraction of the total population may be in the excited state during laser pumping. As a result, the ground rovibronic state may be depleted or *bleached* when molecules that have been excited do not readily return to their original ground state. In the case of strong bleaching, the balanced cross-rate model [16],

$$N_u + N_l \cong N_l^0, \tag{12}$$

where $N_l^0$ is the initial population in level $l$, becomes inaccurate. These depleting processes would include (*i*) efficient photo-dissociation or photo-ionization from the excited state, (*ii*) quenching to slowly-relaxing vibrational levels, and (*iii*) slow ground-state RET. For OH, RET in the ground state appears fast enough to keep level $l$ populated [29]. However, Vibrational Energy Transfer (VET) is slow (in comparison to $Q_e$) in the ground electronic state [30]; consequently, molecules that are quenched to $v'' > 0$ do not readily return to $v''=0$ [20, 31].

## 2 Experiments

### *2.1 Apparatus*

To stabilize a flame at atmospheric pressure and above, we used a sintered bronze water-cooled flat-flame (McKenna) burner with a 2.5 cm diameter. The burner was mounted on a 2-D traversing mechanism, which employed computer-interfaced stepper motors. The flow of gases was metered with Linde electronic mass flow

controllers; these were also connected (through an RS–232 port) to an IBM-compatible PC, employing a menu-driven interface program. Most of the measurements described below were performed at atmospheric pressure. However, those at high pressure employed our high-pressure facility [32].

The second harmonic of a Quanta-Ray DCR–3G Nd:YAG laser was used to pump a PDL–2 dye laser. The output of the dye laser was frequency doubled (in a WEX–1) and tuned to the $Q_1(8)$ transition of OH ($\lambda = 309.3$ nm). The horizontally-polarized beam (preferable for minimum Rayleigh scattering) was focused over the burner with a 500 mm focal length lens; this resulted in a beam waist of $\approx 220$ μm. After the burner, the UV beam was collimated and a portion was sent to a photodiode, which was used to monitor shot-to-shot energy fluctuations. This detector was also used to find the position of the beam relative to the burner. The fluorescence was collimated with a 250 mm focal length, plano-convex lens, rotated by 90° with two mirrors, attenuated when necessary with neutral density filters (to stay within the 0.5 V linear range of the photomultiplier tube), and focused at the monochromator entrance slit with a 300 mm focal length, plano-convex lens. The resulting spatial resolution was about 80 μm × 1.7 mm, with the minor dimension along the burner streamwise (vertical) direction. We employed a 0.5 m monochromator with gratings blazed at 250 nm and 1 μm. The grating blazed at 1 μm was used in third order, and though its efficiency was less than that of the other grating, it was preferable for the narrow-band measurements because of its higher dispersion. For the narrow-band measurements, the monochromator was tuned to the $P_1(9)$ transition ($\lambda = 312.5$ nm), and the exit slit was opened to 200 μm. For wide-band operation, the monochromator was tuned to be middle of the $R_1$ and $R_2$ branches (307.1 nm), and the exit slit was opened to 1 mm. The resulting 1.6 nm bandpass allowed us to capture most of the $R_1$- and $R_2$-branch fluorescence, while rejecting the scattered radiation. Excluding the different grating efficiencies, the wide-band fluorescence signals were about 5.5 times greater than the equivalent narrow-band values.

The laser system was set to deliver two equal-intensity pulses, separated by $\approx 4.5$ ns and each having a 2.5 ns FWHM. With a UV-beam energy of $\approx 10$ mJ, a laser spectral width of $\approx 0.7\ \mathrm{cm}^{-1}$ (FWHM, estimated from laser absorption measurements), and a spot size of $\approx 200$ μm, we estimate a peak spectral irradiance of $7 \times 10^9\ \mathrm{W/cm^2 \cdot cm^{-1}}$. To resolve the temporal characteristics of the fluorescence pulse, we used an RCA 1P28 photomultiplier tube, with a specially-designed voltage divider circuit [33]. This was used in conjuction with a Stanford Research Systems SR255 fast sampler, with its 500 ps gate placed at the peak of the first fluorescence pulse. For accurate triggering of the fast sampler, we relied on the signal from a second photodiode. The fluorescence voltages were then digitized and stored on an IBM-compatible PC with the SR245/SR265 computer interface/software. Typically, for each spatial location, we used 400 individual laser shots to obtain an average fluorescence voltage.

Potential sources of measurement bias include fluorescence vignetting (resulting from the burner occluding the fluorescence cone) and self-absorption. To eliminate the vignetting of the fluorescence profile, we blocked the lower half of the fluorescence beam when sampling near the burner surface. In addition, the self-absorption was reduced by decreasing the length of flame crossed by the fluorescence; that is, we sampled near the burner edge for the highest concentrations of OH. For measurements further from the flamefront, we progressively translated the burner horizontally to move closer to the centerline, thus minimizing edge effects on the measured profiles. As an example, for measurements at a height of $y = 0.5$ mm, the distance from the burner centerline was 8.5 mm, while for those at $y = 9$ mm, the distance from the centerline was only 2 mm. This set of burner movements was facilitated by a modification of the SR265 software that allowed programmed movement of the burner (or other) stepper motors between data points.

### 2.2 Results and Discussion

To investigate the robustness of the wide-band technique, we compared the wide-band results with those using the narrow-band saturated fluorescence method. The following parameters were varied to obtain a range of conditions:

1. the equivalence ratio from $\varphi = 0.6$ to 1.6;
2. the cold-gas velocity from $v_c = 10.4$ cm/s to 31.2 cm/s;
3. the $N_2$ dilution – the ratio of $N_2$ to $O_2$ flow rates – from $\psi = 0$ to 4;
4. the pressure from 1 bar to 10 bar.

The resulting flames are described in Table 2.

The fluorescence measurements were calibrated using laser absorption in a lean flame ($\varphi = 0.8$, $\psi = 3.1$,

**Table 2.** Description of flames used in experiments[a]

| Variable | $\varphi$ | $\psi$ | $v_c$ [cm/s] | $P$ [bar] |
|---|---|---|---|---|
| $v_c$ | 0.8 | 3.1 | 10.4 | 1 |
| | 0.8 | 3.1 | 15.6 | 1 |
| | 0.8 | 3.1 | 20.8 | 1 |
| | 0.8 | 3.1 | 31.2 | 1 |
| $\varphi$ | 0.6 | 3.1 | 10.3 | 1 |
| | 1.0 | 3.1 | 10.4 | 1 |
| | 1.2 | 3.1 | 10.3 | 1 |
| | 1.4 | 3.1 | 10.4 | 1 |
| | 1.6 | 3.1 | 10.4 | 1 |
| $\psi$ | 0.8 | 4.0 | 12.6 | 1 |
| | 0.8 | 2.0 | 7.8 | 1 |
| | 0.8 | 0.0 | 3.0 | 1 |
| $P$ | 0.8 | 3.1 | 26.4 | 1 |
| | 0.8 | 3.1 | 13.2 | 2 |
| | 0.8 | 3.1 | 6.6 | 4 |
| | 0.8 | 3.1 | 6.6 | 6 |
| | 0.8 | 3.1 | 4.9 | 8 |
| | 0.8 | 3.1 | 3.9 | 10 |

[a] The cold-gas velocity is derived using a temperature of 298 K and the flame pressure

$v_c = 10.4$ cm/s) at a height of 1 mm above the burner surface. We scanned the laser over selected transitions and in each case recorded the total absorption. These values along with the temperature (measured with a miniature thermocouple) and the absorption path length were necessary to obtain the absolute OH number density. We determined the absorption path length from a horizontal profile, at a height of 1 mm, of the relative OH concentration. Since the horizontal profile is biased by fluorescence trapping when detecting the $P_1(9)$ transition, we tuned the monochromator to the satellite $O_{12}(10)$ line. This significantly reduces self-absorption, since the transition probability of this line is down by a factor of $\approx 30$ (from the value for the $P_1(9)$ line). The same fluorescence calibration factor was then used for all the flames, since the sensitivity of the saturated fluorescence to quenching is small ($\approx 18\%$ for the narrow-band measurements). Thus, a two-fold increase in quenching reduces the fluorescence by only $\approx 15\%$. By probing the $f_1(8)$ state, we also reduced the senstivity of the fluorescence measurements to the Boltzmann fraction: with respect to the calibration condition ($T = 1750$ K), the variation in Boltzmann fraction is only $+0.5\%$ to $-10\%$ over the range of 1100 K to 2400 K.

In Fig. 3 we compare the narrow- and wide-band measurements for a variation in the cold-gas velocity. By varying the total flow rate at constant stoichiometry and dilution ($\varphi = 0.8$ and $\psi = 3.1$), we increase the burnt-gas temperature, from 1750 K at a cold-gas velocity of $v_c = 10.4$ cm/s to $\approx 2100$ K at $v_c = 31.2$ cm/s. At $v_c = 31.2$ cm/s, the cold-gas velocity is approaching its adiabatic limit; this introduces some instability in the flame, as is apparent from the increased measurement scatter compared to that observed at lower cold-gas velocities. Typically, the burner was *zeroed* (with respect to the beam) before each profile; the repeatability of this process ($\approx 25$ μm) along with the repeatability and long term stability of the flames led to some difference in the wide- and narrow-band concentrations for $y \leq 0.7$ mm. Another noticeable difference is the small decrease ($\approx 100$ μm) in flame stand-off distance in going from cold-gas velocities of $v_c = 10.4$ cm/s to 31.2 cm/s [34]. On

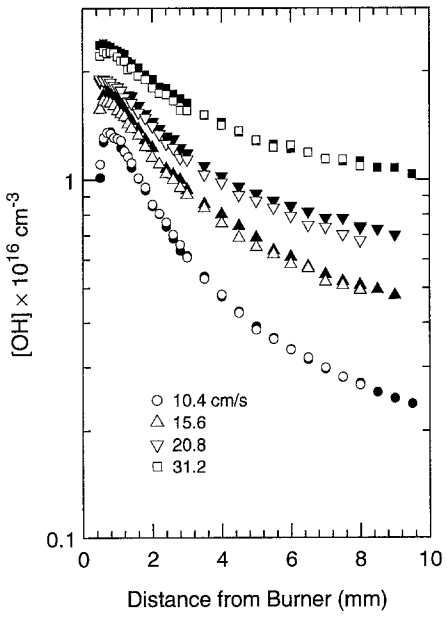


**Fig. 3.** [OH] vs distance from the burner for a variation in cold-gas velocity (see Table 2). Measurements with the wide-band technique are represented with the open symbols, while those with the narrow-band technique are shown with the closed symbols. The respective calibration factors for the wide- and narrow-band measurements were derived from the flame with $v_c = 10.4$ cm/s

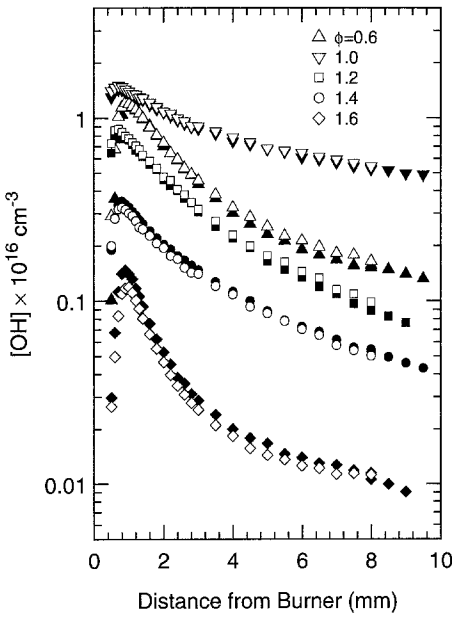


**Fig. 4.** [OH] vs distance from the burner for a variation in equivalence ratio (see Table 2). Measurements with the wide-band technique are represented with the open symbols. For clarity, the calibration flame ($\varphi = 0.8$) has been omitted

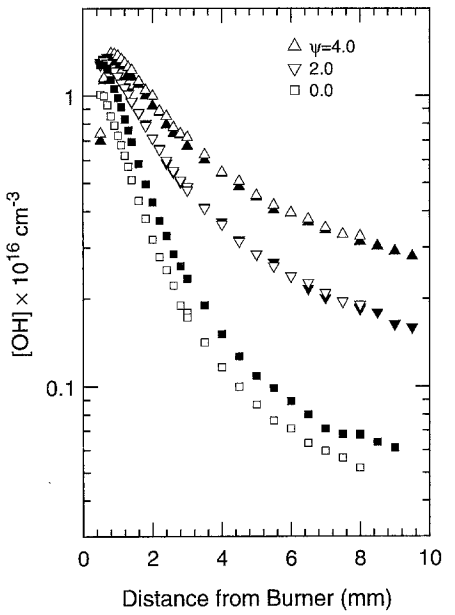


**Fig. 5.** [OH] vs distance from the burner for a variation in dilution (see Table 2). Measurements with the wide-band technique are represented with the open symbols. For clarity, the calibration flame ($\psi = 3.1$) has been omitted

the whole, the comparison between the narrow- and wide-band measurements is excellent, both throughout each flame and from one flame to the next.

In the next set of measurements (Fig. 4), we compare the two methods for changes in equivalence ratio from 0.6 to 1.6 (while holding constant $\psi$ and $v_c$). As with the previous set, the comparison is very good throughout the range of equivalence ratios. One advantage of narrow-band detection is that it offers excellent discrimination against interfering signals (scattered light, fluorescence, etc.). Nonetheless, even with wide-band detection in the flame at $\varphi = 1.6$, we observe no significant difference in the two profiles, thus indicating no significant interference even at low concentrations ($10^{14}$ cm$^{-3}$). In addition to fluorescence interferences (from hydrocarbons in rich flames), one might expect interferences from laser scattering and rotational-Raman scattering [8]. However, Rayleigh and Raman scattering interferences have been greatly reduced with horizontally-polarized radiation.

Over the range of conditions studied, we expect that a variation in the dilution ratio could produce the largest difference in the fluorescence yield between the wide- and narrow-band measurements. This is based on experiments showing that $N_2$ has a large cross section for rotational energy transfer [35–38], but a small cross section for electronic quenching [25]. In Fig. 5 we show [OH] profiles with $\varphi = 0.8$ and dilutions of $\psi = 4.0$, 2.0, and 0.0; to obtain these flames, we simply reduced the $N_2$ flow rate while keeping the other flow rates constant. With less dilution the flame moves closer to the burner and the burnt-gas temperature increases, though this latter effect is mitigated by increased heat loss to the burner. Another significant difference among the profiles is the ratio of [OH] at the peak to that at $y = 9$ mm. While the peak [OH] values are about the same among the four flames, the equilibrium values drop significantly with decreasing dilution, in spite of the greater burnt-gas temperature. At $\psi = 4.0$ the wide-band values are about 5% above the narrow-band measurements; at $\psi = 0.0$ the wide-band results are 20–25% below the corresponding narrow-band values. The electronic quenching rate coefficient increases by a factor of $\approx 4$ from $\psi = 4.0$ to 0.0 (based on the small electronic quenching cross section for $N_2$). If, under these conditions, the net rate for RET did not vary, the steady-state fluorescence yield, as given by $N_A^{ss}/N_u^{ss}$ (9), would drop by $\approx 60\%$ (instead of 25–30%). This may indicate that the net rate coefficient for RET increases somewhat in going from $\psi = 4.0$ to 0.0. In addition, while a decrease in $Q_{r,u}/Q_e$ reduces the *steady-state* fluorescence yield, the increase in $Q_e$ tends to increase the fluorescence yield (perhaps by 10%), since the manifold population is closer to its steady-state value. Accordingly, we observed a temporal shift in the peak signal of 1 ns (to an earlier time) in going from a dilution of 4.0 to 0.0.

Another factor which could mitigate the effects of a large change in $Q_{r,u}/Q_e$ is saturation broadening, the apparent broadening of the transition resulting from the saturation process in concert with the large spectral energy density in the wings of the laser's spectral profile. This is illustrated in Fig. 6 by excitation scans for which the monochromator was set for wide-band operation and

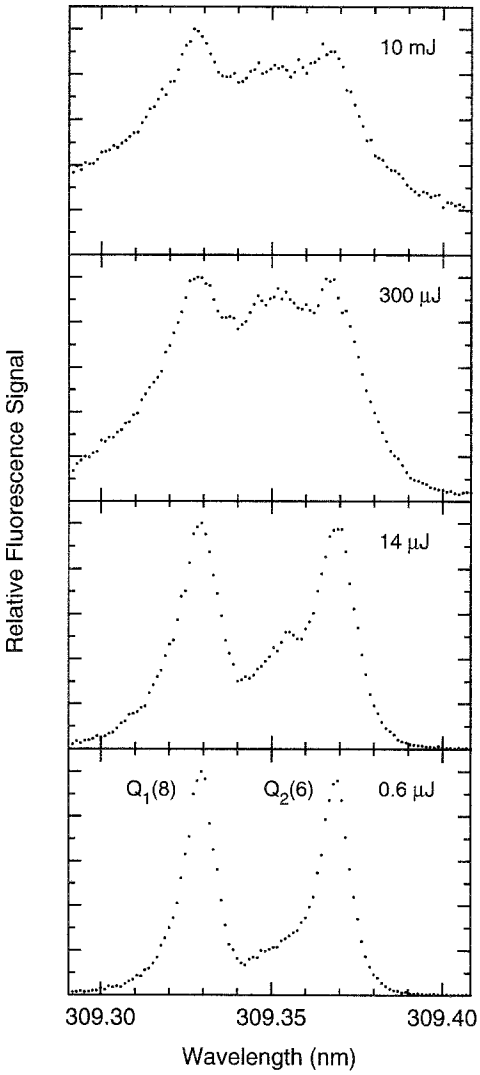


**Fig. 6.** Excitation scans over the $Q_1(8)$ and $Q_2(6)$ lines (as well as the satellite $Q_{21}(8)$ and $Q_{12}(6)$ lines) with various beam energies

the laser wavelength was scanned over the $Q_1(8)$ and $Q_2(6)$ lines (and the satellite $Q_{21}(8)$ and $Q_{12}(6)$ lines). While the laser linewidth was estimated at 0.7 cm$^{-1}$ (FWHM), the absorption linewidth was calculated to be $\approx 0.26$ cm$^{-1}$ (FWHM) using a temperature of 1750 K and the collisional data of Rea et al. [39, 40]. The four scans were obtained by progressively decreasing the laser irradiance using Pyrex plates. With no attenuation, the spectrum is strongly distorted by saturation broadening: at the left edge of the spectrum ($\lambda = 309.29$ nm) the signal is $\approx 40\%$ of the peak value at the $Q_1(8)$ wavelength; in addition, the $Q_{21}(8)$ and $Q_{12}(6)$ satellite lines contribute significantly to the total signal. One result, then, of saturation broadening is that the neighboring transitions are also excited, and this results in an increased $N_A/N_u$, which is then somewhat less sensitive to $Q_{r,u}/Q_e$. Of course, this feature also means that the spectral wings of the beam – like the spatial wings – add a linear component to the saturated portion, thereby increasing the sensitivity of the measurements to quenching (and laser power). These two effects are amplified when (*i*) the

spectral density of lines is large and (*ii*) the lines are strongly broadened. With the narrow-band technique, though, one discriminates against these weakly excited lines by detecting only the directly-excited rovibronic state. The increased sensitivity due to weak excitation of neighboring lines was in fact observed in generating saturation curves (i.e., fluorescence signal versus laser irradiance). For the narrow-band measurements, the sensitivity to the laser irradiance was $\approx 18\%$, while that for the wide-band technique was $\approx 23\%$. This increase in sensitivity could be eliminated by pumping a more isolated line (e.g., the $P_1(5)$ or the $P_1(9)$ line). The two points given above are satisfied for the transitions of NO at pressures of several bar or more. Consequently, we would expect that with wide-band detection, saturation of the NO fluorescence would be difficult at high pressures; this conclusion has been confirmed by the recent measurements of Reisel and Laurendeau [41].

For the final set of data, we measured the OH fluorescence as a function of pressure from 1 bar to 10 bar for wide- and narrow-band conditions at a fixed location 1.5 mm above the burner. While holding the equivalence and dilution ratios constant at 0.8 and 3.1, respectively, we increased the total mass flow with increasing pressure (though the cold-gas velocity decreased with pressure); this, along with a screen placed above the burner, enhanced the flame stability. Because of transient effects, the peak of the fluorescence pulse occurred at earlier times with increasing pressure. For the narrow-band measurements, this shift amounted to $\approx 1.0$ ns in going from 1 bar to 10 bar, while for the wide-band measurements, it amounted to $\approx 2.0$ ns. The additional shift associated with wide-band fluorescence represents the extra time necessary to obtain a steady-state rotational distribution. The temporal fluorescence signals also provide a means of measuring the rate of depletion of the laser-coupled levels. This is illustrated in Fig. 7, where we show average fluorescence profiles at 1 bar and 8 bar using narrow-band detection and an accompanying profile from Rayleigh scattering. These data were generated by scanning the 500 ps gate over the fluorescence (or Rayleigh scattering) pulse. At atmospheric pressure the profile shows no evidence of depletion: the ratio of the peaks is about unity, as would be expected from the irradiance (i.e., Rayleigh scattering) profile. At 8 bar, though, the signal at the second temporal peak has dropped by $\approx 25\%$ relative to signal from the first peak; this reduction in signal, we believe, is due to bleaching of the lower rovibronic level. From these fluorescence profiles, we can estimate the time necessary to obtain a similar depletion in an atmospheric flame. The equivalent number of collisions is found by multiply the time separation of the two peaks, $\approx 4.5$ ns, by the ratio of the pressures, 8. Thus after $\approx 36$ ns, assuming that the transition is saturated during that time, we would expect an $\approx 25\%$ depletion of the ground state.

Figure 8 shows relative signals from wide- ($S_{fW}$) and narrow-band ($S_{fN}$) fluorescence as a function of pressure (where the ratio $S_{fW}/S_{fN}$ is normalized to the value at atmospheric pressure). As before, the comparison shows little difference in the wide- and narrow-band

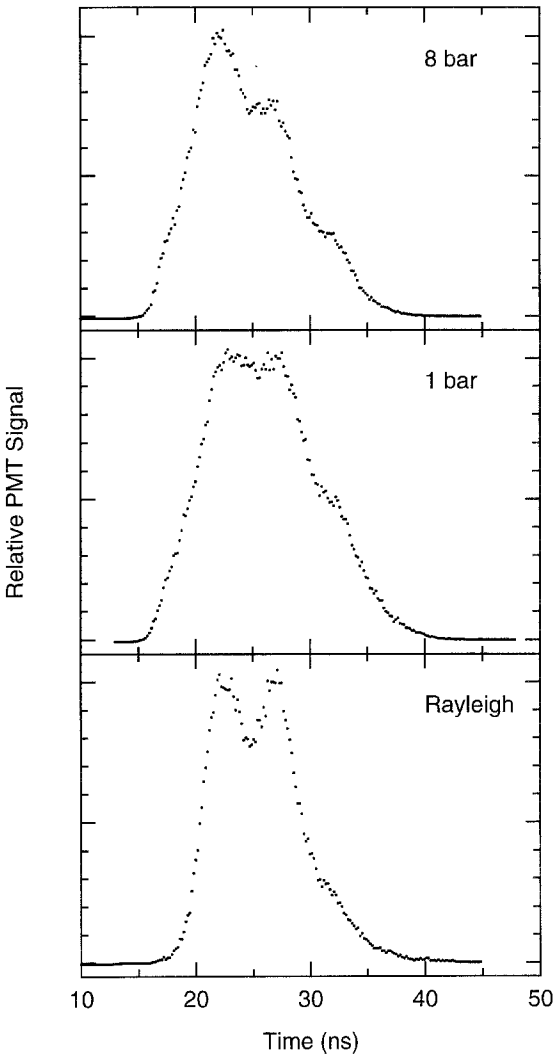


**Fig. 7.** Average temporal profiles for Rayleigh scattering *(bottom)*, for fluorescence from a flame at 1 bar *(middle)*, and for fluorescence from a flame at 8 bar *(top)*. The fluorescence profiles were recorded with narrow-band detection; those using wide-band detection are similar

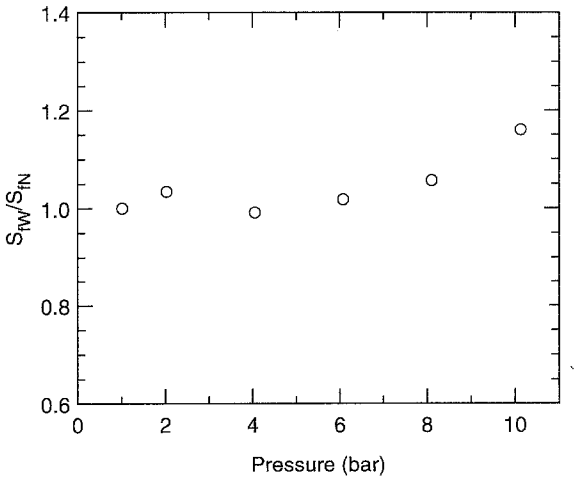


**Fig. 8.** Wide- and narrow-band fluorescence ratio, $S_{fW}/S_{fN}$, vs pressure in the burnt-gas region ($y = 1.5$ mm above the burner) of lean flames (see Table 2)

results. Over this range of conditions ($P=1$ bar to 10 bar and $T=1750$ K), the absorption linewidth varies from $\approx 0.26\,\mathrm{cm}^{-1}$ to $\approx 0.63\,\mathrm{cm}^{-1}$ (FWHM) [39, 40]. However, due to saturation broadening, both the wide- and narrow-band methods should exhibit reduced sensitivity, compared to linear fluorescence, to broadening of the absorption profile. For the wide-band technique, the increase in pressure has two distinct offsetting effects: increased quenching – without increased collisional broadening – decreases the excitation of neighboring lines; however, increased line broadening – without increased quenching – increases the excitation of neighboring lines. The narrow-band technique also shows sensitivity to collisional broadening when the width of the fluorescence line (convolved with the entrance slit function) becomes larger than the exit slit width [10]. Ideally one would have an exit slit width much larger than this convolved line; however, in practice the exit slit width must be set small enough to discriminate against neighboring transitions. Presumably as a result of these offsetting factors, the ratio $S_{fW}/S_{fN}$ is nearly constant. The greates deviation from unity occurs at 10 bar. In this case, the narrow-band measurement was taken out of sequence, and the high value of $S_{fW}/S_{fN}$ may have resulted from misadjustment of the monochromator or the electronics when measuring $S_{fN}$.

Using a monochromator for our wide-band measurements was in part a matter of convenience. However, a monochromator effectively rejects scattering, which is important for measurements in particle-laden flames, near surfaces, and in flames with low hydroxyl concentrations (e.g., in rich flames). In the absence of these difficulties, one can collect the entire (0,0) band without the need of filters [17]. On the other hand, when surface or particle scattering is significant, one can detect fluorescence from the entire (0,1) band, $\lambda \approx 343-358$ nm [42, 43]. This band is much weaker than the (0,0) band, with a relative transition probability of $A_{01}/A_{00} \cong 0.004$ [44]. Nonetheless, with this approach one can easily reject scattering (using a Schott WG–335 color glass filter, for example), and furthermore the fluorescence is not biased by radiative trapping, which can be severe with (0,0) detection in large flames. Ketterle et al. [42] report that with a XeCl-excimer laser and the (0,0)/(0,1) excitation/detection scheme, single-shot 2–D images of OH fluorescence are feasible even without saturation. Another approach for wideband saturated OH fluorescence is to pump a transition in the (1,0) band and to detect the (1,1) and (0,0) bands, while rejecting both (1,0) fluorescence and scattering [18]. Saturation of (1,0) transitions is certainly possible: the ratio of Einstein $B$-coefficient is $B_{lu}(1,0)/B_{lu}(0,0) \cong 0.27$ for the $Q_1(8)$ transition in the (1,0) and (0,0) bands [44]. This approach has the advantage over the former of a much larger fluorescence yield. Unfortunately, because one cannot separate the (0,0) and (1,1) fluorescence bands with filters ($\lambda_{00} \cong 306$–$319$ nm and $\lambda_{11} \cong 312$–$326$ nm), the fluorescence yield will be sensitive to the ratio of vibrational energy transfer ($v'=1 \rightarrow 0$) and electronic quenching, $Q_v/Q_e$, in addition to the ratio $Q_r(u, c)/Q_e$.

## 3 Conclusions

We have compared wide- and narrow-band saturated fluorescence of an $A^2\Sigma^+$-$X^2\Pi(0,0)$ transition of hydroxyl using theory and experiments. From the theoretical development, we find that in general wide-band saturated fluorescence is sensitive to collisions in two ways. First, the steady-state fluorescence yield varies with the ratio of rate coefficients for rotational energy transfer and electronic quenching; this ratio, $Q_r(u, c)/Q_e$, determines the number of neighboring rotational states that are populated during the laser pulse. Only when this ratio is much greater than $1/F_{Bu}$ (where $F_{Bu}$ is the rotational Boltzmann fraction of the excited rovibronic state), will the distribution approximate a Boltzmann distribution. Thus for OH (and for most diatomics under most circumstances), the wide-band fluorescence yield will be sensitive to $Q_r(u, c)/Q_e$. Second, even when this ratio is constant (from one flame condition to the next), the wide-band fluorescence can vary with the total collisional rate coefficient, $\overline{Q}_r(c, u) + Q_e$; only after a sufficient number of collisions, corresponding to $\approx 2.5$ ns for OH in an atmospheric flame, is the rotational manifold near steady state. Saturation also results in broadening of the temporal fluorescence pulse, and thus a 2.5 ns laser pulse (FWHM) at 1 bar is apparently sufficient, though we do not recommend using pulses shorter than this for atmospheric flames.

In the experiments we compared wide-band – detecting the $R_1$ and $R_2$ branches of the (0,0) band – and narrow-band OH fluorescence in a wide variety of premixed atmospheric flames. These included flames for which we varied the equivalence ratio ($\varphi = 0.6$ to 1.6), the total flow rate (and thus the temperature, from about 1750 K to 2100 K), and the $N_2$ dilution ratio ($\psi = 0.0$ to 4.0). In general the derived wide- and narrow-band concentrations were within $\approx 10\%$, throughout each flame and from one flame to the next. Even with small concentrations in the rich flames, where one might expect fluorescence or scattering interferences, the comparison is excellent. The variation in dilution resulted in the most significant difference between the wide- and narrow-band measurements. However, perhaps due to mitigating factors (e.g., weak excitation of neighboring lines), we observed only a 20–25% drop in the wide-band fluorescence (relative to the narrow-band values) in changing the $N_2/O_2$ dilution from 3.1 to 0. An additional difference between the two techniques is the response to saturation broadening: with the wide-band method, weakly excited neighboring transitions are also detected, whereas the narrow-band method discriminates against this linear (or near linear) fluorescence component. This apparently resulted in a measurable increase in the sensitivity of the wide-band fluorescence to laser power; to avoid this increased sensitivity, one should pump a more isolated line (for example, the $P_1(5)$ or the $P_1(9)$ line). In addition we compared wide- and narrow-band measurements in flames at pressures of 2, 4, 6, 8, and 10 bar; as with the atmospheric flames, the two techniques gave about the same result.

The measurements indicate that when applied with caution – that is, appreciating the underlying physical processes – wide-band saturated fluorescence of OH can yield results comparable to the narrow-band method. Saturation offers the advantage of high signals and reduced sensitivity to quenching and laser irradiance, thus making the fluorescence measurement more quantitative. With relaxed detection requirements (a monochromator is no longer necessary), saturated fluorescence can be applied to 2–D regions, assuming one has the requisite laser irradiance. However, our measurements suggest that saturation, when coupled with a long pulse length, may lead to significant bleaching of the ground state at pressures above 1 bar. Consequently for measurements of hydroxyl concentration, the wide-band technique seems particularly well suited to atmospheric flames, where one can take advantage of the longer pulse width and the larger pulse energy of XeCl-excimer lasers.

*Acknowledgments.* This work was supported by the National Aeronautics and Space Administration (Lewis Research Center) and by the U.S. Department of Energy, Office of Basic Energy Sciences, Division of Chemical Sciences.

## References

1. E.H. Piepmeier: Spectrochim. Acta B **27**, 431 (1972)
2. J.W. Daily: Appl. Opt. **16**, 568 (1977)
3. R.P. Lucht, D.W. Sweeney, N.M. Laurendeau: Combust. Flame **50**, 189 (1983)
4. K. Kohse-Höinghaus, W. Perc, J. Just: In *Proc. 20th Symposium (Int'l) on Combustion* (Combustion Institute, Pittsburgh, PA 1984) pp. 1177–1185
5. J.T. Salmon, R.P. Lucht, D.W. Sweeney, N.M. Laurendeau: In *Proc. 20th Symposium (Int'l) on Combustion* (Combustion Institute, Pittsburgh, PA 1984) pp. 1187–1193
6. J.T. Salmon, N.M. Laurendeau: Appl. Opt. **24**, 1313 (1985)
7. P. Desgroux, M.J. Cottereau: Appl. Opt. **30**, 90 (1991)
8. R.P. Lucht, D.W. Sweeney, N.M. Laurendeau: Combust. Sci. Technol. **42**, 259 (1985)
9. C.D. Carter, G.B. King, N.M. Laurendeau: Combust. Sci. Technol. **78**, 247 (1991)
10. C.D. Carter, G.B. King, N.M. Laurendeau: Appl. Opt. **31**, 1511 (1992)
11. P. Desgroux, E. Domingues, M.J. Cottereau: Appl. Opt. **31**, 2831 (1992)
12. A.P. Baronavski, J.R. McDonald: Appl. Opt. **16**, 1897 (1977)
13. L. Pasternack, A.P. Baronavski, J.R. McDonald: J. Chem. Phys. **69**, 4830 (1978)
14. P.A. Bonczyk, J.A. Shirley: Combust. Flame **34**, 253 (1979)
15. R.P. Lucht, N.M. Laurendeau: Appl. Opt. **18**, 856 (1979)
16. R.P. Lucht, D.W. Sweeney, N.M. Laurendeau: Appl. Opt. **19**, 3295 (1980)
17. M. Schäfer, W. Ketterle, J. Wolfrum: Appl. Phys. B **52**, 341 (1991)
18. R.W. Scheffer, M.N. Namazian, J. Kelly: Opt. Lett. **16**, 858 (1991)
19. J.R. Reisel, C.D. Carter, N.M. Laurendeau, M.C. Drake: Combust. Sci. Technol. **91**, 271 (1993)
20. C.D. Carter, J.T. Salmon, G.B. King, N.M. Laurendeau: Appl. Opt. **26**, 4551 (1987)
21. A. Hindmarsh: ACM SIGNUM Newslett. **4**, 4 (1980)
22. R.P. Lucht, D.W. Sweeney, N.M. Laurendeau: Appl. Opt. **25**, 4086 (1986)
23. K. Kohse-Höinghaus, J.B. Jeffries, R.A. Copeland, G.P. Smith, D.R. Crosley: Chem. Phys. Lett. **152**, 160 (1988)
24. G. Zizak, J.A. Lanauze, J.D. Winefordner: Combust. Flame **65**, 203 (1986)
25. N.L. Garland, D.R. Crosley: In *Proc. 21st Symposium (Int'l) on Combustion* (Combustion Institute, Pittsburgh, PA 1986) pp. 1693–1702
26. T. Ebata, Y. Anezaki, M. Fujii, N. Mikami, M. Ito: Chem. Phys. **84**, 151 (1984)
27. Aa. S. Sudbø, M.M.T. Loy: J. Chem. Phys. **76**, 3646 (1982)
28. J.A. Gray, J.L. Durant, P.H. Paul, J.W. Thoman, Jr.: AIAA paper 93-0924 (1993)
29. G. Zizak, G.A. Petrucci, C.L. Stevenson, J.D. Winefordner: Appl. Opt. **30**, 5270 (1991)
30. K.J. Rensberger, J.B. Jeffries, D.R. Crosley: J. Chem. Phys. **90**, 2174 (1989)
31. D.H. Campbell: Appl. Opt. **23**, 689 (1984)
32. C.D. Carter, G.B. King, N.M. Laurendeau: Rev. Sci. Instrum. **60**, 2606 (1989)
33. J.M. Harris, F.E. Lytle, T.C. McCain: Anal. Chem. **48**, 2095 (1980)
34. C. Ferguson, J.C. Keck: Combust. Flame **34**, 85 (1979)
35. R.K. Lengel, D.R. Crosley: J. Chem. Phys. **67**, 2085 (1977)
36. D. Stepowski, M.J. Cottereau: J. Chem. Phys. **74**, 6674 (1981)
37. J. Burris, J.J. Butler, T.J. McGee, W.S. Heaps: Chem. Phys. **151**, 233 (1991)
38. A. Jörg, U. Meier, R. Kienle, K. Kohse-Höinghaus: Appl. Phys. B. **55**, 305 (1992)
39. E.C. Rea, Jr., A.Y. Chang, R.K. Hanson: J. Quant. Spectrosc. Radiat. Transfer **37**, 117 (1987)
40. E.C. Rea, Jr., A.Y. Chang, R.K. Hanson: J. Quant. Spectrosc. Radiat. Transfer **41**, 29 (1989)
41. J.R. Reisel, N.M. Laurendeau: Combust. Sci. Technol. (in press)
42. W. Ketterle, M. Schäfer, A. Arnold, J. Wolfrum: Appl. Phys. B **54**, 109 (1992)
43. N.M. Laurendeau, J.E.M. Goldsmith: Combust. Sci. Technol. **63**, 139 (1989)
44. I. Chidsey, D.R. Crosley: J. Quant. Spectrosc. Radiat. Transfer **23**, 187 (1979)